Materials and Design 195 (2020) 108907

Contents lists available at ScienceDirect

Materials and Design

journal homepage: www.elsevier.com/locate/matdes

An exploratory study on strengthening and thermal stability of magnetron sputtered W nanoparticles at the interface of Cu/Ni multilayer films

R.L. Schoeppner [a,c,*], G. Mohanty [b,c], M.N. Polyakov [c], L. Petho [c], X. Maeder [c], J. Michler [c]

[a] California Nanosystems Institute, University of California Santa Barbara, Santa Barbara CA, 93106 USA
[b] Materials Science and Environmental Engineering, Tampere University, 33014 Tampere, Finland
[c] Laboratory of Mechanics of Materials and Nanostructures, Empa – Swiss Federal Laboratories for Materials Science and Technology, Feuerwerkerstrasse 39, 3602 Thun, Switzerland

GRAPHICAL ABSTRACT

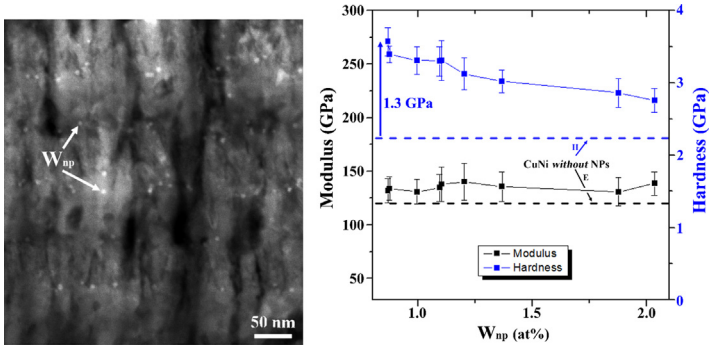

ARTICLE INFO

Article history:
Received 7 January 2020
Received in revised form 8 May 2020
Accepted 20 June 2020
Available online 12 July 2020

Keywords:
Nanoparticles
Multilayers
Strengthening
Nanoindentation
In-situ XRD

ABSTRACT

An initial study to investigate the effect of controlled deposition of nanoparticles at multilayer interfaces was conducted to explore the mechanical effect of particles on laminate structures. Nanoparticles with diameter of about 4.5 nm were specifically deposited at the interface between Cu and Ni laminates by forced agglomeration of magnetron sputtered ions using a Mantis Ltd. Nanogen50 nanoparticle generator and the hardness of these films were measured using the nanoindentation technique. Cu/Ni laminates *without* W nanoparticles have an average modulus value of approximately 120 ± 3.7 GPa and hardness value of 2.23 ± 0.07 GPa, while the hardness values of the particle-containing films are greater, regardless of particle density. The areas with the lowest particle density at the interfaces (0.9 at.% W) show the greatest increase in hardness, with an increase of about 1.3 GPa greater than the particle-free sample. However, as the particle density increases, there is a corresponding decrease in hardness. In-situ x-ray diffraction of these films was also conducted to observe the annealing behavior of these films. For all samples, the Cu and Ni layered structure remained intact; however, there is evidence of Ni diffusion along grain boundaries and interaction with the oxygen, likely creating NiO. After annealing, a significant number of the W nanoparticles dissolved into the Ni matrix to create NiW solid-solution. The ability to deposit particles with such precise control has the potential to open up an exciting new field of research.

* Corresponding author at: California Nanosystems Institute, University of California Santa Barbara, Santa Barbara CA, 93106 USA.
E-mail addresses: r.l.schoeppner@gmail.com, rlschoeppner@ucsb.edu (R.L. Schoeppner).

https://doi.org/10.1016/j.matdes.2020.108907

1. Introduction

Many techniques are used to increase the strength of a material depending on the application and desired results. Some of these techniques include the control of grain size [1–3], deposition of nanolaminate structures [4,5], and the addition of precipitates or hard particles [6–8]. Refining grain size to increase yield strength in severe plastically deformed ultrafine grained metals [9] and electrodeposited nanocrystalline metals [10] is already being extensively explored. Incorporating hard particles or precipitates into a material is a well-known and widely practiced method for strengthening materials, often used in precipitation strengthened aluminum, advanced steels and super alloys. These particles act as barriers to dislocation motion as well as Frank-Read dislocation sources [11], which increases both the strength and strain-hardening ability of the material. Most of the particle-strengthened materials in use today are bulk metals where precipitation and oxide dispersion strengthening has shown significant strengthening effects and increased thermal stability [12,13].

In bulk metallic systems, deconvoluting the contribution of various strengthening mechanisms in a laboratory scale is not straightforward as it is very difficult to vary one parameter while keeping the others constant. For example, it can be difficult to change the grain size while keeping the precipitate size constant. However, thin films deposited by magnetron sputtering offer greater variability and control of various microstructural parameters. In case of laminate strengthening, the individual layer thickness and composition can be controlled precisely. Multiple specimens having varying layer thicknesses can be produced to study the effect of individual layer thickness towards strengthening.

With recent advances in materials design that constantly push the mechanical requirements of thin films and coatings, one question to explore is if it is possible to combine both laminate and particle strengthening. While adding the particles in the matrix itself will be beneficial, as known from precipitation and dispersion strengthened alloys, very few experimental studies have investigated the effect of particles that are deposited at the multilayer interface [14]. Tayyebi and Eghbali investigated a Cu/Ni/Al layered microstructure with ceramic reinforcement particles fabricated using accumulative roll bonding; however, the evolution of the microstructure described in the study starts with layer thinning followed by discontinuity of the layers and finally even distribution of particles and enhanced bonding of the layers which lead to increased strength. Due to the continually evolving microstructure, the strengthening effect of the nanoparticles in particular was not discussed. Other investigations have focused on the effect of particles on the strength of nanolaminate structures [15,16]. One atomistic simulation study focused on particle interactions within multilayers and suggested a significant effect of these particles on the strength of incoherent interface multilayers [15], focusing more specifically on the effect of particles within one of the layers. Another study investigated how interfacial steps and imperfections of Cu/Nb multilayer films affect the strengthening as the step size and density of the imperfection increases [17]. These two results suggest that the addition of particles at the interfaces of laminate films could have a profound effect on the strength of laminate films.

Traditionally, particles are distributed into the material either by precipitation from a solid solution [11], ball milling for dispersion of oxide particles [18,19] or, as in this study, by direct physical deposition. The method used in this study to incorporate hard particles into the film is physical deposition by forced agglomeration of sputtered atoms, also known as inert gas condensation. The method has been used to create free nanoparticles for a variety of different optical and catalytic applications [20,21]; however, no research has yet been conducted using this source to incorporate size specific particles at predetermined locations in the coating. To date, this type of strengthening has only been applied to the matrix of select alloys and oxide dispersion strengthened materials. With no investigations focusing on the combined effect of particles distributed at the interface of nanolaminate films, we aim to explore a new class of nanocomposite materials that can be fabricated by sputtering a matrix and co-sputtering particles, enabling virtually any combination of materials that can be sputtered. For simplicity, this study starts with the controlled deposition of nanoparticles at multilayer interfaces to enable a fundamental study of the strengthening effect of particles on laminate structures and thermal stability of these particle-reinforced composites. The main focus of this investigation is to observe the interaction of hard particles deposited at the usually coherent interface of Cu/Ni nanolaminate films, specifically utilizing a combinatorial design approach to quickly investigate the effect of nanoparticle concentration on the performance of these laminate films.

2. Experimental

Cu/Ni multilayer films were deposited using a customized QPREP 500 PVD chamber by Mantis Deposition Ltd. onto a <100> oriented Si substrate. The Si substrate was lowered 8 cm from the normal deposition position, where all the targets are normally focused to deposit at the center of the substrate, to create a range of layer thicknesses on a single wafer. The Cu and Ni targets were oriented at 180° from one another, which produces linear layer thickness gradients across the wafer, while the nanoparticle source was oriented at 90° from each of the other targets to create a particle density gradient perpendicular to the layer thickness gradient (Fig. 1). Two different wafers were produced for

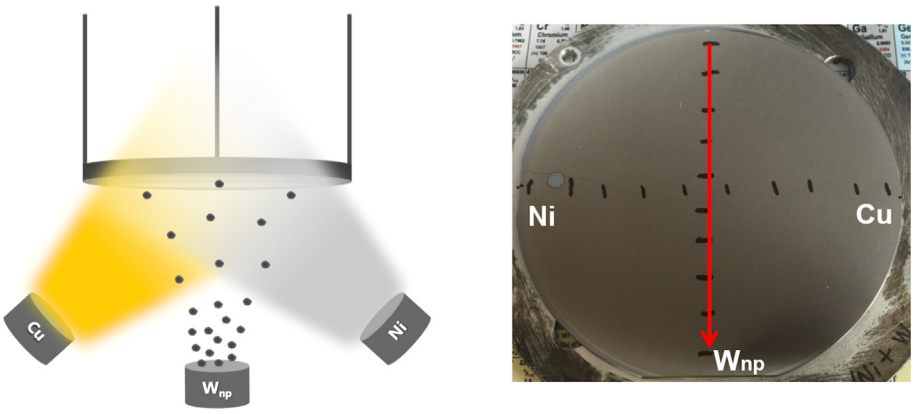

Fig. 1. Schematic of the lowered deposition technique used to create the layer thickness and W_{np} concentration gradient across the wafer (left). Each target is angled at 90 degrees from each other to create higher concentrations of Cu, Ni, and W_{nps} at the different edges (left). The indented region along the centerline of the wafer (red arrow) corresponds to layer thicknesses of 85 nm Cu and 55 nm Ni for both samples, with and without nanoparticles. (For interpretation of the references to colour in this figure legend, the reader is referred to the web version of this article.)

Table 1
Physical measurements sample summary from XRF characterization.

Sample name		Total thickness (μm)	Centerline Cu layer thickness (nm)	Centerline Ni layer thickness (nm)	Centerline Total W concentration (at.%)
Cu/Ni *without* W_{np}		3.62 ± 0.01	91 ± 0.05	53 ± 0.06	n/a
Cu/Ni *with* W_{np}	Low	1.55 ± 0.003	78 ± 0.23	61 ± 0.26	0.9 ± 0.1
	High	1.58 ± 0.003	86 ± 0.12	55 ± 0.13	2.0 ± 0.1

this investigation: a Cu/Ni multilayer film with individual layer thicknesses ranging from 50 to 150 nm with a total of 20 bilayers and a second wafer deposited with a total of 10 bilayers and the addition of W nanoparticles deposited at each Ci-Ni interface. Each Cu layer was deposited with 5.5e-3 mTorr while the Ni layer with 8.0e-3 mTorr. The particles were produced using a Nanogen50 nanoparticle generator from Mantis Ltd. and filtered using the MesoQ nanoparticle mass filter to specifically deposit W nanoparticles with a nominal 4.5 nm diameter at the interfaces. The nanoparticle current measured passing through the MesoQ was approximately 0.2 nA for each half hour deposition at the interface. Since this wafer was also deposited in the lowered configuration, the nanoparticle density also varies across the wafer. To verify the individual layer thicknesses, total film thickness, and approximate W nanoparticle density, x-ray fluorescence (XRF) was used to measure the at.% of each constituent, as well as the total film thickness, using a Fischerscope x-ray XDV with a W source and acceleration voltage of 30 kV. A summary of the locations investigated with corresponding Cu layer thickness, Ni layer thickness, and estimated W nanoparticle spacing is presented in Table 1. X-ray diffraction (XRD) maps of both wafers were obtained using a Bruker D8 device equipped with a copper source and using the Bragg Brentano configuration with 1 mm point focus. A scan from 2theta 20° to 100° was conducted at each measurement location. This was followed by in-situ XRD while annealing the samples using an Anton Paar DHS 1100 chamber at temperatures from 100 °C to 400 °C in 100 °C increments of 40 min duration under slight vacuum (approximately 1e-3 mbar; heating rate between the temperature increments of 10 °C per minute) to track microstructural changes occurring in the system as a result of annealing.

Nanoindentation of the as-deposited films with and without W nanoparticles was performed with a Berkovich diamond tip using an UNHT^3 Anton Paar nanoindentation system [22]. The principle of UNHT^3, unlike most nanoindentation systems, is based on the idea of using two independent vertical axes: one for indentation and the other for active surface referencing. The differential displacement between the indenter and the reference is measured as the depth of penetration, which results in low thermal drift and high stability in measurements. Both films were indented using load-controlled indentation profile that comprised of loading at 30mN/min, hold of 10s at peak load of 10mN followed by complete unloading at 30mN/min. The maximum depth of displacement was approximately 15% of film thickness in both cases to avoid some substrate effects [23]. Indents were performed along the centerline of the wafer, which corresponds to layer thicknesses of approximately 85 nm Cu and 55 nm Ni to compare the mechanical properties with and without W nanoparticles. A total of more than 250 indents were performed with at least 25 indents every 1 cm of the wafer area to obtain appropriate statistics for each nanoparticle density.

Cross-sectional transmission electron microscopy (TEM) samples were prepared by a focused ion beam (FIB) liftout technique using a Vela FIB (TESCAN) and attached to Cu TEM grids. Microstructural characterization of these film cross-sections was carried out using a JEM2200fs TEM (JEOL), and a Titan Themis TEM equipped with a SuperEDX system (FEI) was also used for Electron dispersive x-ray (EDX) analysis.

3. Microstructural characterization

3.1. XRF mapping across thickness gradients

XRF mapping was conducted across the wafer to determine total thickness and individual layer thicknesses of the samples were calculated based on composition and total thickness. Fig. 2a and b show the Cu and Ni layer thicknesses across the wafer determined by XRF for the (a) Cu/Ni *without* nanoparticles sample and (b) Cu/Ni sample *with* W nanoparticles, showing similar layer thicknesses across the wafer. The red bar in the Cu/Ni with Wnp shows the section of the wafer that was indented as well as the XRF measurement area for determining the Wnp concentration (Fig. 2c). This also corresponds to the red arrow shown in Fig. 1(b) that shows the indented region along the centerline of the wafer.

The individual layer thicknesses for both of the samples show linear trends, with Cu increasing from 45 to 140 nm and Ni decreasing from 100 to 30 nm (measuring left to right). The W signal from the interfacial particles in the second sample (Fig. 2c), which was measured along the center of the sample perpendicular to the changing Cu and Ni layer thickness gradient (highlighted in red), shows a changing particle

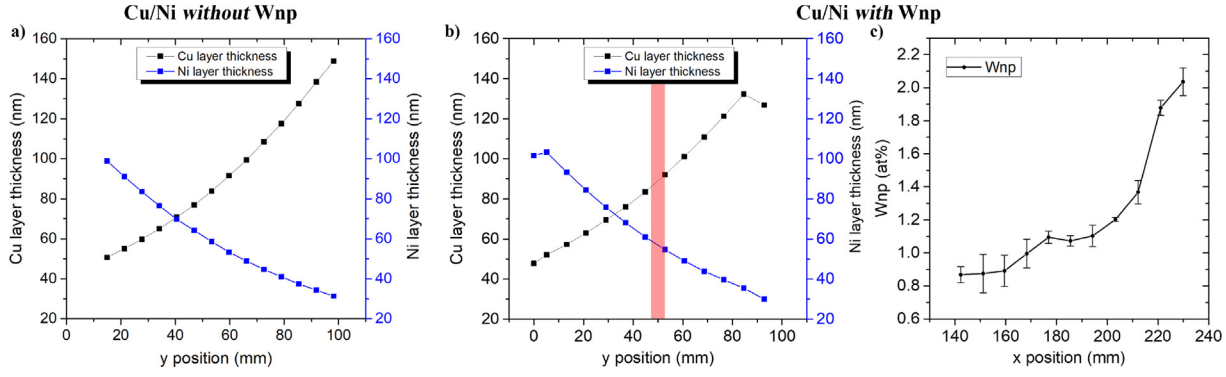

Fig. 2. XRF summary of Cu/Ni multilayers without (a) and with (b/c) W nanoparticles at the interfaces. The nanoparticle concentration varies across the wafer, with a sharp increase in 20% of the wafer closest to the nanoparticle source, as seen in (c). The determined error for the layer thicknesses (a/b) are within the size of the data marker. The indented region along the centerline of the wafer corresponds to layer thicknesses around 85 nm Cu and 55 nm Ni for both samples, with and without nanoparticles.

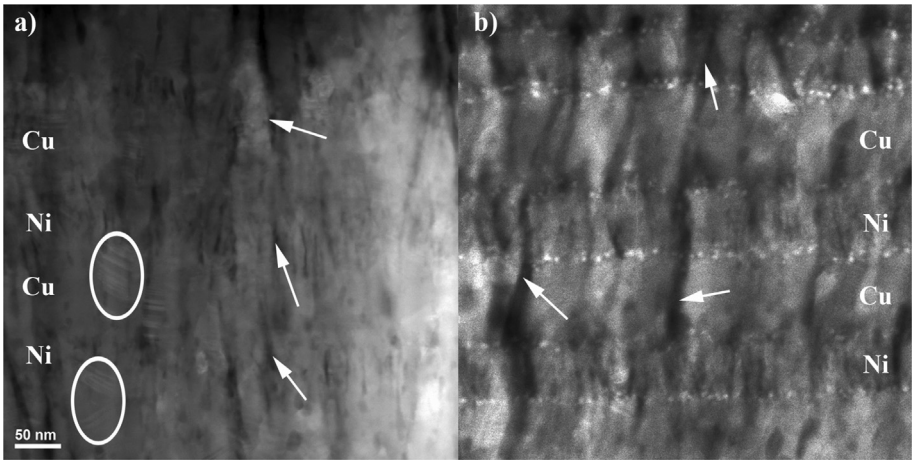

Fig. 3. DF-STEM images of CuNi multilayer films without (a) and with (b) nanoparticles deposited at the interfaces. Examples of growth twins are highlighted inside the circles and intergranular pores with arrows.

concentration across the wafer, with the highest concentration of particles located approximately 20% from the edge of the wafer that was closest to the nanoparticle source. This higher concentration at the edge of the wafer is due to the particle stream coming out of the small 5 mm aperture of the particle generator. According to Mantis Ltd., the nanoparticle source deposits in a bell-curve distribution with a width dependent on the distance from the particle generator, combining that with the lowered substrate deposition technique offset, the peak particle density occurs closer to the particle gun, as shown in Fig. 1b.

3.2. Scanning transmission electron microscopy (STEM)

Microstructural characterization of these nanolaminate films was conducted using scanning-TEM (STEM) to determine particle distribution and interface morphology. Cross-sectional lamellae were removed from the center of the Cu/Ni nanolaminate and along the centerline of the Cu/Ni nanoparticle-containing nanolaminate on both the low (approx. 0.9 at.% W) and high (approx. 2.0 at.% W) particle density sides of the wafer. Dark-field (DF)-STEM images were obtained for similar layer thickness combinations and two different nanoparticle density conditions, in order to examine microstructural and interfacial changes stemming from the addition of nanoparticles at the interface. The Cu/Ni nanolaminate without particles is compared to the high particle density laminate in the DF-STEM images in Fig. 3, which emphasize mass and thickness variations. The oblique orientation during deposition led to shadowing during grain growth, resulting in the observed intergranular pores, which can also occur when films are deposited at higher processing pressures [24]. It is important to note that these pores are present in both samples and in similar percentages (4.8 ± 1.9%, 6.8 ± 3.0%, and 6.7 ± 2.9% for particle-free, low density, and high density samples, respectively calculated from TEM images) regardless of nanoparticles at the interface and so are not expected to affect the observed hardness relationship.

All samples showed some evidence of growth twins in the Cu layers, with slightly more observed in the nanoparticle-free samples. Similar growth twins, present only in Cu layers, have been observed in Cu/Ni multilayers having individual layer thickness >25 nm [25]. Twinning has been shown to increase the strength, ductility, and thermal stability of materials [26–28]. From previous studies, Cu samples that have nanotwins with a similar twin spacing (7 nm) as observed in our Cu/Ni sample have a tensile strength approximately 600 MPa higher than a twin-free sample [29], suggesting that the presence of the growth twins will contribute to additional strengthening in the coatings beyond that expected from nanolaminate or nanocrystalline strengthening.

In Fig. 4, the increased particle spacing is easily noticeable when comparing the low-density (Fig. 4a) to the high-density (Fig. 4b) areas. Since these lamellae are approximately 100 nm thick, the projected particle spacing observed in the high-density sample is not the actual spacing of the particles on the interface and while there might be some particles that were deposited on top of each other, it is

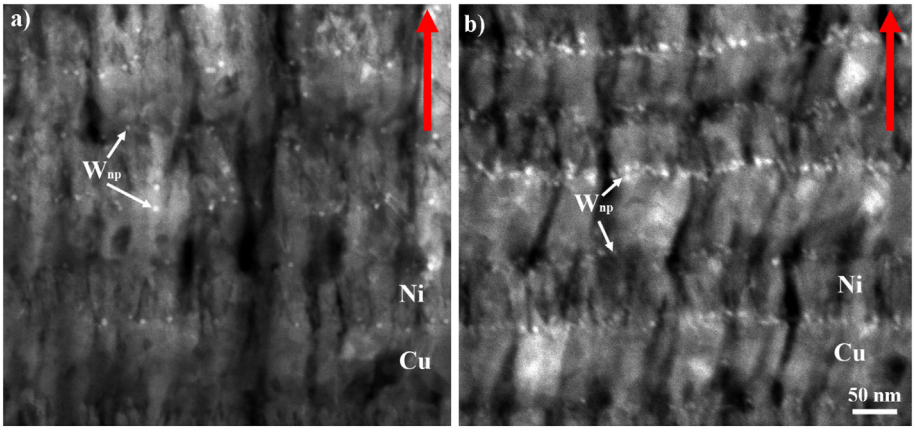

Fig. 4. DF-STEM images of low particle density (a) and high particle density (b) areas of the coating, showing a distinct difference in nanoparticle density between the two areas of the film. The growth direction of the film is indicated by the two arrows.

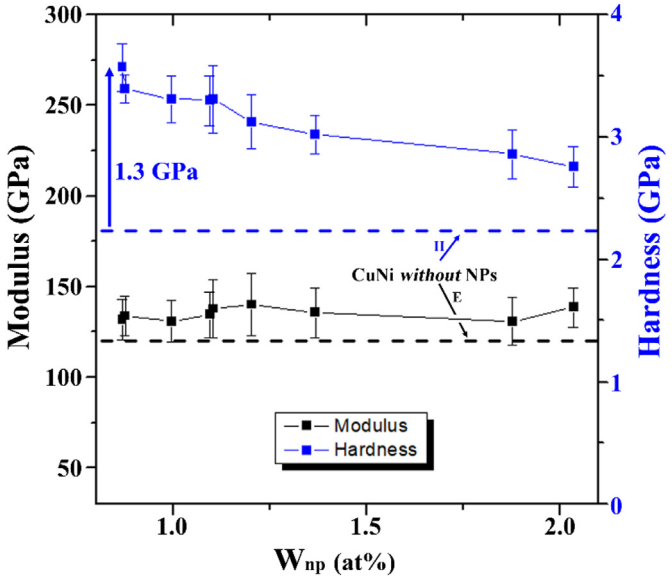

Fig. 5. Nanoindentation results as a function of position across substrate, along the changing nanoparticle density direction. Dotted lines signifying the modulus (black) and hardness (blue) values of Cu/Ni without W_{np} are shown for comparison. (For interpretation of the references to colour in this figure legend, the reader is referred to the web version of this article.)

not expected to be a majority. While the particle density seems to show a dependence on which layer the nanoparticle were deposited onto, this is most likely due to a difference in the main chamber pressure during deposition, which has since shown to affect the particle density that can reach the substrate.

4. Mechanical characterization using nanoindentation

Both nanolaminate films were indented across the changing particle density concentration and constant layer thicknesses of around 85 nm Cu and 55 nm Ni, as previously described in Table 1. Unsurprisingly, the Cu/Ni *without* W_{np} sample showed no dependence on the indentation position along the wafer, with an average modulus value of approximately 120 ± 3.7 GPa and hardness value of 2.23 ± 0.07 GPa. When compared to other studies, the hardness values seem to compare closely with the other reported values, with Cu/Ni 55 nm spacing having a H_{IT} of about 3.5 GPa [25].

Fig. 5 shows a summary of the measured modulus and hardness values of the particle-strengthened nanolaminate sample as a function of particle density. The dashed lines in the figure are the average values for the particle-free film to use as a visual comparison for the film with interfacial particles. For all particle concentrations, the hardness of the particle-containing film is greater than the coating without interfacial particles, regardless of particle density. However, the areas with the lowest particle density at the interfaces show the greatest increase in hardness, about 1.3 GPa higher than the particle-free sample. The moduli of the two films are approximately the same, within the spread of the measurements, which is expected as the elemental ratios of Cu/Ni and the texture of the films remain approximately constant.

5. In-situ XRD investigation at elevated temperatures

An in-situ XRD experiment was conducted on each of the samples to determine if the nanoparticles facilitated in stabilizing the microstructure at temperatures up to 400 °C. Tracking the diffraction peaks of the Cu and Ni peaks at each temperature could help to show if there is a retardation of Cu and Ni grain growth or alloying due to the addition of interfacial particles. Fig. 6 shows the summary of the diffraction evolution as temperature increases for the Cu/Ni nanolaminate *without* particles and for the low-density Cu/Ni *with* W_{np}. From A room temperature scan was conducted before and after the heating cycle to compare peak ratios and determine the extent of alloying.

Rietveld refinement [30] was conducted on the Cu and Ni (111) peaks, showing an approximate crystallite size of 20 nm for both Cu and Ni. These values are consistent between samples and are, therefore, independent of nanoparticle concentration. Both films seem to respond similarly to annealing, with little change up to 300 °C. After 300 °C, the films start showing a reduced Ni (111) signal, which continues to drop as the temperature is increased further. Post-anneal room temperature scans show an approximately 50% drop in the Ni (111) signal, either indicating alloying or oxidation of the Ni as well as a shift in the Cu and Ni peaks, which suggests a change in the internal stresses after annealing. Closer examination of the lattice parameters of the as-deposited Cu and Ni peaks show a deposition stress of 600 MPa for the particle-free samples, and − 300 MPa for the low-density sample. After annealing, the films have developed additional compressive stresses, as can be seen from the peak shift in room temperature XRD spectra.

To examine the extent of alloying, if any, TEM lamellae were prepared from annealed films to examine the microstructure in more detail

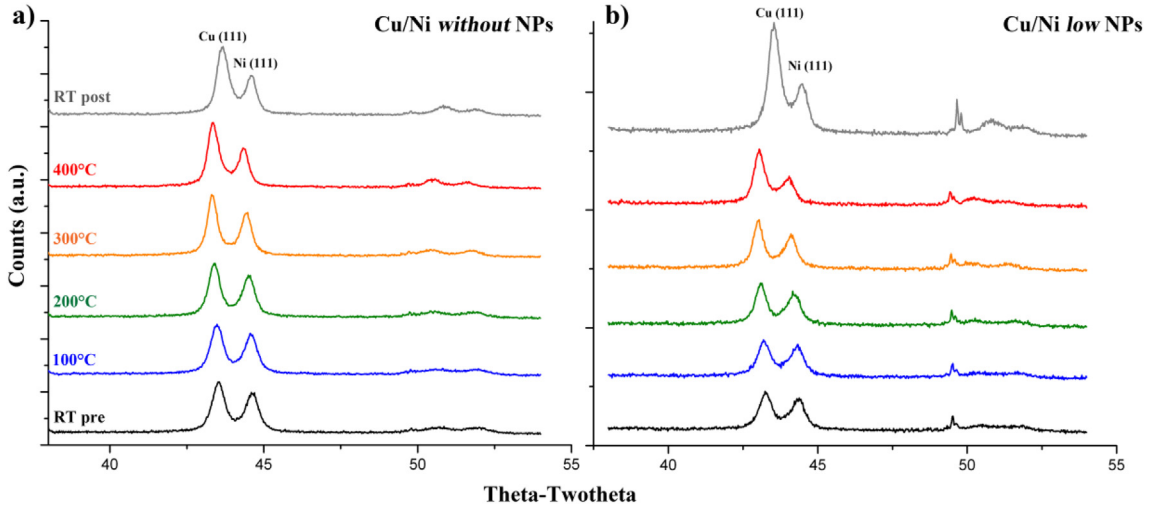

Fig. 6. Diffraction peaks resulting from in-situ annealing of the low nanoparticle concentration (right) and particle-free samples (left).

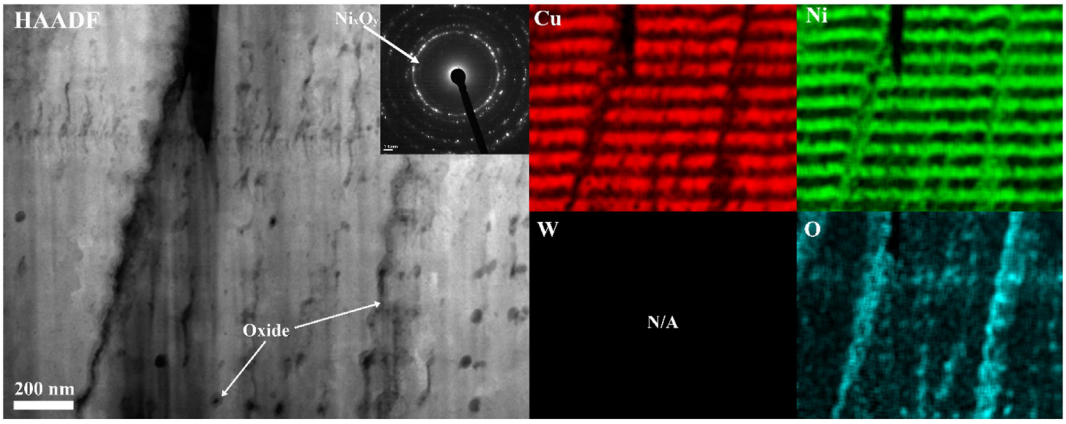

Fig. 7. Cross-sectional STEM EDX scan of Cu/Ni without W_{np} sample annealed to 400 °C during in-situ XRD experiments, 9 pixel averaged at.% maps. An extremely faint diffraction ring from NixOy formation is visible in the HAADF inset, highlighted with an arrow.

and investigate if the nanoparticles reacted with either of the constituents. Fig. 7 is an EDX at.% map of the Cu/Ni nanolaminate *without* W_{np} annealed up to 400 °C, with individual Cu, Ni, W, and O elements separated into individual frames. This particular section contained large intergranular pores throughout the thickness of the film, which facilitated the diffusion of oxygen from the surface deep into the film (lower right frame). In general, the Cu and Ni layers remained intact; however, there is evidence of Ni diffusion along grain boundaries and interaction with the oxygen, likely creating a NiO. This is particularly evident around the pores and along the large intergranular pores (indicated by the arrows in the HAADF image).

A similar cross-section of the Cu/Ni low particle density annealed sample was examined, with the elemental maps shown in Fig. 8. Similar to the Cu/Ni *without* particles, this coating also showed substantial oxidation at the intergranular pores and interfacial pores. There also seems to be a greater concentration of Ni diffusion into the Cu layer, specifically at the grain boundaries, which then interacted with the oxygen to create a significant amount of NiO at the grain boundaries and pores. Close examination of the HAADF image on the left of the figure shows that there are still some W nanoparticles which have not reacted with the other elements in the coating; however, the density when compared to the pre-annealed sample is much less, suggesting that the majority of the nanoparticles have dissolved into the matrix, to create a NiW solid-solution. Under very close examination, this is also apparent in the W concentration map showing the majority of the W signal in the Ni layer.

Finally, the annealed high particle density sample EDX maps are shown in Fig. 9. The majority of the features are quite similar to the other two films, with Ni and O concentrated at the grain boundaries and pores, Ni and Cu interdiffusion along grain boundaries, and a significant amount of W_{np} dissolved into the Ni layer, likely creating a NiW solid-solution. However, with this sample, there does seem to be a more pronounced localization of W remaining at the interfaces, along with a higher concentration of O, which is also reflected in the HAADF image. It is difficult to determine if this is an indication of a W_xO_y at the interface or a complex Ni-W-O oxide. Closer scrutiny of the HAADF image reveals much darker (lower atomic mass) layers after each Cu layer that were not present in the pre-annealed images and is not present in either of the other annealed samples. Since there was a higher density of W particles at this interface in the pre-annealed samples, as was discussed previously, this is a good indication that this layer is likely some form of a W_xO_y.

6. Discussion

While Cu/Ni multilayers can often consist of coherent and semi-coherent interfaces with a (111) out of plane crystal orientation, the multilayers in this study, both with and without nanoparticles at the interface, show no significant presence of epitaxial growth between Cu and Ni layers. This is likely due to the presence of oxygen in the deposition chamber (due either to a small leak in the chamber or insufficient

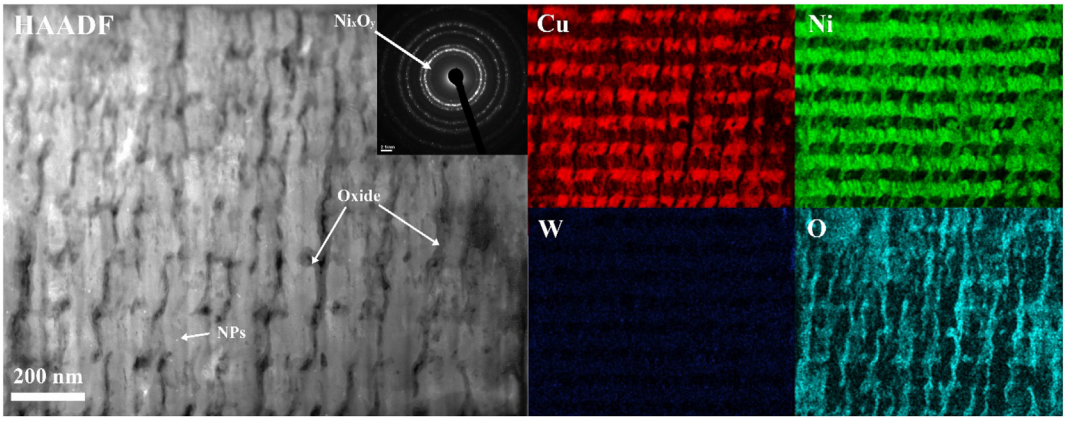

Fig. 8. Cross-sectional STEM EDX scan of Cu/Ni with W_{np} (low) sample annealed to 400 °C during in-situ XRD experiments, 9 pixel averaged at.% maps. An extremely faint diffraction ring from NixOy formation is visible in the HAADF inset, highlighted with an arrow.

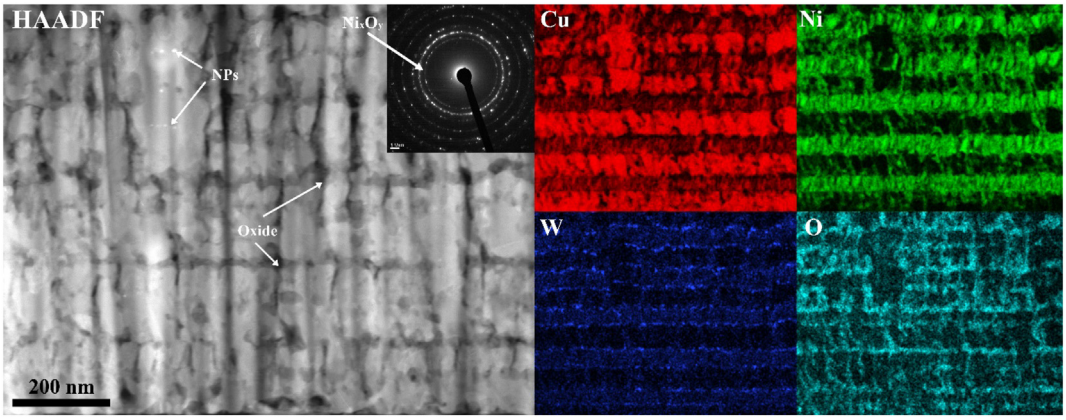

Fig. 9. Cross-sectional STEM EDX scan of Cu/Ni with W_{np} (high) sample annealed to 400 °C during in-situ XRD experiments, 9 pixel averaged at.% maps An extremely faint diffraction ring from NixOy formation is visible in the HAADF inset, highlighted with an arrow.

base pressure when starting deposition) or due to the Cu and Ni interruptions during the nanoparticle deposition, which allows for a small buildup of oxide on the fresh surface. In general, the nanoparticle addition to the multilayers does not seem to greatly affect either the layered structure, the amount of porosity observed in the films, or the out-of-plane texture of the individual layers.

Porosity in the films is expected to decrease the hardness of the Cu/Ni multilayer films reported in this study. It will be instructive to compare the hardness of the baseline sample – Cu/Ni multilayer without W_{np} – with literature to understand the extent of hardness drop due to porosity. Majority of previous studies on Cu/Ni multilayers have focused on identical individual layer thickness for both Cu and Ni layers and have not reported the grain sizes which makes a direct comparison with our films difficult. Liu et al. [25] have reported hardness values of Cu/Ni multilayers with individual layer thickness varying from 1 to 200 nm and for two different orientations: (100) and (111). The hardness of (111) Cu/Ni multilayer with 50-70 nm individual layer thickness, closest to our films, is ~3.5 GPa [25]. The hardness of (100) Cu/Ni multilayer with similar layer thickness was found to be lower at ~2.7 GPa. Since our Cu/Ni multilayer films have a very strong (111) texture, we expect the hardness values to be more closer to 3.5 GPa than 2.7 GPa. Zhu et al. [31] have reported hardness values of 2.1 and 5.5 GPa for monolayer (111) Cu and (111) Ni films, respectively. Using a simple rule-of-mixtures for Cu/Ni multilayer studied herein yields hardness value of ~3.35 GPa which matches reasonably well with those reported by Liu et al. for (111) texture. These hardness values are substantially higher than our Cu/Ni multilayer films that exhibit a hardness of 2.23 GPa. Therefore, porosity seems to affect the hardness of the Cu/Ni multilayers substantially.

The model proposed by Chen et al. [32] correlates the mechanical properties of porous and dense materials. This model was used to perform a first order porosity estimation for Cu/Ni multilayer used in this study. If we assume that the hardness of ~3.4 GPa reported in literature corresponds to a dense film and our hardness measurements to correspond to a porous film, we obtain a porosity estimate of ~15% for Cu/Ni multilayers using this model. This estimate matches reasonably well with the initial porosity estimates of ~5–10% from TEM image analysis. It should be noted that the model proposed by Chen et al. [32] is accurate within a 5–7% porosity estimate window. While porosity does affect the hardness values of the films studied herein, similar pore densities in the films will make relative changes in hardness comparable. The TEM images show similar pore densities in all the films, with slightly lower porosity (~5%) for the W-free Cu/Ni film compared to W-containing films (~7%). If the observed hardness changes were solely due to porosity, then we should have observed lower hardness in the W containing films. Even if we assume that our porosity estimates for the different films are not correct and that there is a 5% porosity change between two films, the resultant change in hardness will be only ~400 MPa. This is much smaller than the observed difference of ~1.3 GPa between CuNi multilayers with 0.9% W_{np} and without W_{np}. Therefore, porosity in the films cannot explain the strengthening in W-containing Cu/Ni films.

Another important consideration when discussing hardness of thin films are residual stresses. Residual stresses have been shown to alter the measured nanoindentation hardness values by as much as ~22% [33]. A first order estimation of the residual stresses in the three films (no W_{np}, low W_{np} and high W_{np} content) was calculated from the XRD data to estimate the influence of these residual stresses on the measured hardness values. Tsui, Oliver and Pharr [33] showed residual stress can affect the hardness of an aluminum alloy by ~6% for ~300 MPa compressive residual stress and by ~22% for 300 MPa tensile residual stress under biaxial conditions. Since the residual stress in multilayer thin films will be mostly bi-axial, this comparison was found to be the most appropriate. Tsui et al. report that the observed change in nanoindentation hardness (and modulus) values as a function of applied (uniaxial and bi-axial) stresses in the material is primarily due change in pile-up behavior of the indents that drastically changes the contact area of indentation. If the correct contact areas are used in mechanical property calculations, then it was found that both hardness and modulus values do not change as a function of applied stress in the material. Using the data from Tsui et al., a first order estimation of the residual stress and corrected hardness of our samples is shown in Table 2, assuming similar extent of pile up for the calculated residual stresses.

The observed trend in hardness actually accentuates when the pile up correction due to residual stress is applied. This strongly suggests that the trends in hardness that we observe in this study (due to W_{np} addition at the Cu/Ni multilayer interface) are real and not due to residual stresses and consequently pile up during indentation in the films. It

Table 2
First-order residual stress calculations from XRD measurements and potential corrrected in hardness due to pile-up effects.

Sample	Residual stress (MPa)	Measured hardness (GPa)	Corrected hardness (GPa)
Cu/Ni without W_{np}	−540	2.2	1.86
Cu/Ni with low W_{np}	+330	3.5	4.3
Cu/Ni with high W_{np}	−130	2.75	2.6

Please note that '−' sign denotes compressive residual stress and '+' sign denotes tensile residual stress.

should be noted that the corrected hardness values reported in the last column should be considered as the "worst-case scenarios" for hardness values. However, severe pile-up was not observed in TEM cross-sections of an indent in the current study. TEM images of the indents were capped with Pt layer before lift-out, preserving the pile-up, if any. No significant pile-up was observed. An image of a TEM lamellae showing no pile-up around the indent is included in supplementary information.

Multiple strengthening mechanisms can be active in multilayer films. For layer thicknesses >50 nm, hardness increases linearly with $h^{-1/2}$ consistent with Hall-Petch relation. However, this will remain similar across all films since they have similar layer thicknesses and grain sizes. TEM investigation of the samples show that the Cu and Ni grain sizes are on the order of the layer thickness or smaller and mostly consist of re-nucleated grains every layer. The Cu grain size varies between 20 and 80 nm while Ni is on the order of 20 nm. Due to smaller grain sizes, coherency stresses (another multilayer strengthening mechanism) are unlikely to develop in these films. Since all the films show similar texture, any change resulting from that can be ruled out as well. Elastic modulus mismatch remains similar for all films as well. Therefore, only the presence of the nanoparticles at the interfaces seems to be contributing to the increased hardness of the nanolaminates. This confirms the hypothesis that controlled deposition of nanoparticles can effectively strengthen multilayer structures. However, it is apparent that it does not follow typical strengthening trends for a particle reinforced matrix, where there is a positive correlation between hardness and particle density. Particles in the matrix can act as dislocation barriers, requiring a larger Orowan stress to propagate dislocations [11], followed by the particles acting as Orowan sources [11,34], increasing the number of dislocations in the material and leading to strain-hardening. However, the opposite effect was observed here, where the higher particle density actually results in lower hardness values and therefore, smaller amount of strengthening. This seems to suggest there are two competing deformation mechanisms: one that increases the strength of the nanolaminate and one that leads to increased dislocation motion.

The only discernable difference between the Cu/Ni multilayer films is the presence of W nanoparticles at the interface. Since the layer interface can act as both the source and sink for dislocations, altering the interface will drastically change the dislocation behavior within the individual layers. It is plausible that addition of W nanoparticles to the interface blocks dislocation motion and changes the resulting pile-up behavior at the interfaces – another strengthening mechanism active in multilayer systems with layer thickness >50 nm. It is also possible that the W nanoparticles pin down the smaller nanocrystalline grain boundaries in Cu and Ni inhibiting grain boundary sliding. W in solid solutions has been shown to pin down grain boundaries effectively in nanocrystalline metals [35]. Grain boundary diffusion is important for both intragranular dislocation generation and annihilation as well as grain boundary sliding [36] and has been shown to facilitate both these mechanisms. Depositing W nanoparticles at the interfaces is akin to decorating some of the grain boundaries, that are at the interface, with an immobile particle that blocks grain boundary diffusion and consequently, limits plastic deformation resulting in increases strengthening.

Another possible explanation could be due to strengthening from interfacial imperfections. In a study from 2014, Abdolrahim et al. [37] showed that interfacial imperfections in nanolaminates could lead both to additional strengthening beyond a perfect interface, depending on the size of the imperfection (or step height), as well as softening, depending on the density of these imperfections [17]. In these molecular dynamic simulations, it was shown that the addition of a single "step" imperfection makes dislocation nucleation from this imperfection difficult and increases the strength of the film by approximately 1 GPa due to the increased barrier for dislocation transmission into the second layer. The authors also showed that increasing the density of ledge imperfections at the interface led to a reduction in the strength of the system, which they attributed to the high stress concentrations at the ledges. If the particles create stress fields in the surrounding material, similar to the interface imperfections, then it could explain why there is an initial increase in hardness followed by a slight drop in hardness as the concentration of nanoparticles increases. It should be noted that these do not take a solute or nanoparticle at the interface into account. The influence of a W nanoparticle is likely to be much more severe than an interface imperfection like a ledge or a step. Since this is the first study of its kind, it is too early to conclude on the strengthening mechanism responsible for hardness trends observed in this study.

In-situ XRD annealing of these films shows no obvious difference in the diffraction peaks between the particle-reinforced samples and the particle free multilayers in the theta-two theta scans. However, there was a distinct change in the microstructure of the particle-containing films after annealing, specifically the disappearance of the W nanoparticles for both of the samples, with a few remaining particles in the high concentration sample. According to the accompanying EDS maps, the W particles dissolved into the Ni grains and grain boundaries due to the solubility of W into Ni. The resulting solid-solution strengthening could be beneficial to the overall strength; however, that would remove the particle strengthening benefit observed in this study. Due to surface oxidation of the films, nanoindentation was not performed and the amount of solid-solution strengthening versus particle strengthening was not determined in this study. Therefore, it is important to be careful in the selection of the particle element to avoid this result if the material is to be used at elevated temperatures.

7. Summary

A new deposition technique was utilized to create nanolaminate films with W particles specifically at each interface to investigate the effect of particle density on the mechanical and structural properties of the films. The addition of nanoparticles to the interfaces in a nanolaminate increases the strength of the film system without significantly changing the microstructure of the material.

Small additions of particles are able to increase hardness of the coatings by more than 1 GPa above that of particle-free multilayers. However, at higher particle densities the hardness begins to decrease again, indicating there is likely an ideal particle concentration that would lead to the highest increase in hardness. This was attributed to competing mechanisms where the particles act both as dislocation sources and barriers to dislocation transmission into the other layer. Initial in-situ XRD heating experiments show the W nanoparticles can dissolve into the Ni layer to create a solid-solution Ni—W layer and react with oxygen. This opens up the ability to use nanoparticles to counteract thermal softening that is often seen in multilayers and leads to decreased performance of these coatings over time, leading the way for expansion into other material system combinations and opening up an exciting field of research – investigating strengthening mechanisms and thermal stability of nanoparticle strengthened laminate coatings.

Supplementary data to this article can be found online at https://doi.org/10.1016/j.matdes.2020.108907.

Author contributions

R. Schoeppner: Visualization; Conceptualization; formal analysis; investigation; methodology; data curation; writing-original draft; writing- review & editing.

G. Mohanty: Formal analysis; investigation; methodology; data curation; writing- original draft; writing-review & editing.

M. Polyakov: Formal analysis; investigation; methodology;

L. Petho: Supervision; resources;

X. Maeder: Formal analysis; investigation; methodology; data curation;

J. Michler: Project administration; resources; supervision;

Declaration of competing interest

The authors declare that they have no known competing financial interests or personal relationships that could have appeared to influence the work reported in this paper.

Acknowledgements

The authors would like to acknowledge funding from the EMPA Postdoc program co-funded by FP7: Marie Curie Actions. Further funding was obtained from the EMPAPOSTDOCS-II programme, which received funding from the European Union's Horizon 2020 research and innovation programme under the Marie Skłodowska-Curie grant agreement number 754364.

Data availability

The raw/processed data required to reproduce these findings cannot be shared at this time due to technical or time limitations; however, can be made available upon request.

References

[1] H. Yu, Y. Xin, M. Wang, Q. Liu, Hall-Petch relationship in Mg alloys: a review, J. Mater. Sci. Technol. 34 (2018) 248–256, https://doi.org/10.1016/j.jmst.2017.07.022.
[2] N.J. Petch, Cleavage strength of polycrystals, J. Iron Steel Inst. (1953) 25–28.
[3] E.O. Hall, The deformation and ageing of mild steel: III discussion of results, Proc. Phys. Soc. B. (1951) 747.
[4] J. Wang, Q. Zhou, S. Shao, A. Misra, Strength and plasticity of nanolaminated materials, Mater. Res. Lett. 5 (2017) 1–19, https://doi.org/10.1080/21663831.2016.1225321.
[5] R.L. Schoeppner, N. Abdolrahim, I. Salehinia, H.M. Zbib, D.F. Bahr, Elevated temperature dependence of hardness in tri-metallic nano-scale metallic multilayer systems, Thin Solid Films (2014) 31–36, https://doi.org/10.1016/j.tsf.2014.05.031.
[6] M.A. Muñoz-Morris, C. Garcia Oca, D.G. Morris, An analysis of strengthening mechanisms in a mechanically alloyed, oxide dispersion strengthened iron aluminide intermetallic, Acta Mater. 50 (2002) 2825–2836, https://doi.org/10.1016/S1359-6454(02)00101-5.
[7] N. Fuschillo, M.L. Gimpl, Electrical and tensile properties of Cu-ThO2, Au-ThO2, Pt-ThO2 and Au-Al2O3, Pt-Al2O3 alloys, J. Mater. Sci. 5 (1970) 1078–1086.
[8] S. Tang, T. Xin, W. Xu, D. Miskovic, G. Sha, Z. Quadir, S. Ringer, K. Nomoto, N. Birbilis, M. Ferry, Precipitation strengthening in an ultralight magnesium alloy, Nat. Commun. 10 (2019) https://doi.org/10.1038/s41467-019-08954-z.
[9] R.Z. Valiev, Y. Estrin, Z. Horita, T.G. Langdon, M.J. Zehetbauer, Y. Zhu, Producing bulk ultrafine-grained materials by severe plastic deformation: ten years later, Jom 68 (2016) 1216–1226, https://doi.org/10.1007/s11837-016-1820-6.
[10] C.A. Schuh, T.G. Nieh, H. Iwasaki, The effect of solid solution W additions on the mechanical properties of nanocrystalline Ni, Acta Mater. 51 (2003) 431–443, https://doi.org/10.1016/S1359-6454(02)00427-5.
[11] G. Dieter, Mechanical Metallurgy, 1st Ed1986 pg. 183-186.
[12] R.L. Schoeppner, R.S. Goeke, N.R. Moody, D.F. Bahr, Mechanical and electrical performance of thermally stable Au–ZnO films, Acta Mater. 91 (2015) 1–9, https://doi.org/10.1016/j.actamat.2015.03.024.
[13] G. Robert Odette, N.J. Cunningham, T. Stan, M. Ershadul Alam, Y. De Carlan, Nano-oxide dispersion-strengthened steels, Struct. Alloy. Nucl. Energy Appl, Elsevier 2019, pp. 529–583, https://doi.org/10.1016/B978-0-12-397046-6.00012-5.
[14] M. Tayyebi, B. Eghbali, Microstructure and mechanical properties of SiC-particle-strengthening tri-metal Al/Cu/Ni composite produced by accumulative roll bonding process, Int. J. Miner. Metall. Mater. 25 (2018) 357–364, https://doi.org/10.1007/s12613-018-1579-6.
[15] N. Abdolrahim, I.N. Mastorakos, H.M. Zbib, Precipitate strengthening in nanostructured metallic material composites, Philos. Mag. Lett. 92 (2012) 597–607, https://doi.org/10.1080/09500839.2012.704153.
[16] R.L. Schoeppner, A.A. Taylor, M.J. Cordill, H.M. Zbib, J. Michler, D.F. Bahr, Precipitate strengthening and thermal stability in three component metallic nanolaminate thin films, Mater. Sci. Eng. A 712 (2018) https://doi.org/10.1016/j.msea.2017.11.062.
[17] N. Abdolrahim, I.N. Mastorakos, S. Shao, D.F. Bahr, H.M. Zbib, The effect of interfacial imperfections on plastic deformation in nanoscale metallic multilayer composites, Comput. Mater. Sci. 86 (2014) 118–123, https://doi.org/10.1016/j.commatsci.2014.01.045.
[18] D.. Ying, D.. Zhang, Processing of Cu–Al2O3 metal matrix nanocomposite materials by using high energy ball milling, Mater. Sci. Eng. A 286 (2000) 152–156, https://doi.org/10.1016/S0921-5093(00)00627-4.
[19] C. Suryanarayana, N. Al-Aqeeli, Mechanically alloyed nanocomposites, Prog. Mater. Sci. 58 (2013) 383–502, https://doi.org/10.1016/J.PMATSCI.2012.10.001.
[20] M. Haro, V. Singh, S. Steinhauer, E. Toulkeridou, P. Grammatikopoulos, M. Sowwan, Nanoscale heterogeneity of multilayered Si anodes with embedded nanoparticle scaffolds for li-ion batteries, Adv. Sci. (2017) https://doi.org/10.1002/advs.201700180 1700180. 1700180.
[21] H.A. Ahmed, S.I. Abu-Eishah, A.I. Ayesh, S.T. Mahmoud, Synthesis and characterization of Cu-doped TiO_2 thin films produced by the inert gas condensation technique, J. Phys. Conf. Ser. 869 (2017) https://doi.org/10.1088/1742-6596/869/1/012027.
[22] M. Conte, G. Mohanty, J.J. Schwiedrzik, J.M. Wheeler, B. Bellaton, J. Michler, N.X. Randall, Novel high temperature vacuum nanoindentation system with active surface referencing and non-contact heating for measurements up to 800 °C, Rev. Sci. Instrum. 90 (2019).
[23] R. Saha, W.D. Nix, Effects of the substrate on the determination of thin film mechanical properties by nanoindenation, Acta Mater. 50 (2002) 23–38.
[24] J.A. Thornton, High rate thick film growth, Annu. Rev. Mater. Sci. 7 (1977) 239–260.
[25] Y. Liu, D. Bufford, H. Wang, C. Sun, X. Zhang, Mechanical properties of highly textured Cu/Ni multilayers, Acta Mater. 59 (2011) 1924–1933, https://doi.org/10.1016/j.actamat.2010.11.057.
[26] A.M. Hodge, Y.M. Wang, T.W. Barbee, Large-scale production of nano-twinned, ultrafine-grained copper, Mater. Sci. Eng. A 429 (2006) 272–276, https://doi.org/10.1016/J.MSEA.2006.05.109.
[27] X. Zhang, A. Misra, H. Wang, M. Nastasi, J.D. Embury, T.E. Mitchell, R.G. Hoagland, J.P. Hirth, X. Zhang, A. Misra, H. Wang, M. Nastasi, J.D. Embury, T.E. Mitchell, R.G. Hoagland, Nanoscale-twinning-induced strengthening in austenitic stainless steel thin films, Appl. Phys. Lett. 84 (2004) 1096–1098, https://doi.org/10.1063/1.1647690.
[28] O. Anderoglu, A. Misra, H. Wang, X. Zhang, O. Anderoglu, A. Misra, H. Wang, X. Zhang, Thermal stability of sputtered Cu films with nanoscale growth twins, J. Appl. Phys. 103 (2008) https://doi.org/10.1063/1.2913322 094322-1-094322–6.
[29] L. Lu, Y. Shen, X. Chen, L. Qian, K. Lu, Ultrahigh strength and high electrical conductivity in copper, Science 304 (2004) 422–426, https://doi.org/10.1126/science.1092905.
[30] P. Thompson, D.E. Cox, J.B. Hastings, Rietveld refinement of Debye-Scherrer synchrotron X-ray data from Al2O3, J. Appl. Crystallogr. 20 (1987) 79–83.
[31] X.Y. Zhu, X.J. Liu, R.L. Zong, F. Zeng, F. Pan, Microstructure and mechanical properties of nanoscale Cu/Ni multilayers, Mater. Sci. Eng. A 527 (2010) 1243–1248, https://doi.org/10.1016/j.msea.2009.09.058.
[32] X. Chen, Y. Xiang, J.J. Vlassak, Novel technique for measuring the mechanical properties of porous materials by nanoindentation, J. Mater. Res. 21 (2006) 715–724, https://doi.org/10.1557/jmr.2006.0088.
[33] T.Y. Tsui, W.C. Oliver, G.M. Pharr, Influences of stress on the measurement of mechanical properties using nanoindentation: part I. Experimental studies in an aluminum alloy, J. Mater. Res. 11 (1996) 752–759.
[34] Z. Zhang, D.L. Chen, Consideration of Orowan strengthening effect in particulate-reinforced metal matrix nanocomposites: a model for predicting their yield strength, Scr. Mater. 54 (2006) 1321–1326, https://doi.org/10.1016/J.SCRIPTAMAT.2005.12.017.
[35] T.J. Rupert, J.C. Trenkle, C.A. Schuh, Enhanced solid solution effects on the strength of nanocrystalline alloys, Acta Mater. 59 (2011) 1619–1631, https://doi.org/10.1016/j.actamat.2010.11.026.
[36] G. Mohanty, J.M. Wheeler, R. Raghavan, J. Wehrs, M. Hasegawa, S. Mischler, L. Philippe, J. Michler, Elevated temperature, strain rate jump microcompression of nanocrystalline nickel, Philos. Mag. 95 (2015) 1878–1895, https://doi.org/10.1080/14786435.2014.951709.
[37] N. Abdolrahim, H.M. Zbib, D.F. Bahr, Multiscale modeling and simulation of deformation in nanoscale metallic multilayer systems, Int. J. Plast. 52 (2014) 33–50, https://doi.org/10.1016/j.ijplas.2013.04.002.